Article

α-Tocopherol Is Well Designed to Protect Polyunsaturated Phospholipids: MD Simulations

Xiaoling Leng,[1] Jacob J. Kinnun,[1] Drew Marquardt,[2,3] Mikel Ghefli,[4] Norbert Kučerka,[5,6] John Katsaras,[7,8,9] Jeffrey Atkinson,[4] Thad A. Harroun,[2] Scott E. Feller,[10] and Stephen R. Wassall[1,*]

[1]Department of Physics, Indiana University-Purdue University Indianapolis, Indianapolis, Indiana; [2]Department of Physics, Brock University, St. Catharines, Ontario, Canada; [3]Institute of Molecular Biosciences, University of Graz, Graz, Austria; [4]Department of Chemistry, Brock University, St. Catharines, Ontario, Canada; [5]Canadian Neutron Beam Centre, National Research Council, Chalk River, Ontario, Canada; [6]Faculty of Pharmacy, Comenius University, Bratislava, Slovakia; [7]Neutron Sciences Directorate, Oak Ridge National Laboratory, Oak Ridge, Tennessee; [8]Joint Institute for Neutron Sciences, Oak Ridge, Tennessee; [9]Department of Physics and Astronomy, University of Tennessee, Knoxville, Tennessee; and [10]Department of Chemistry, Wabash College, Crawfordsville, Indiana

ABSTRACT The presumptive function for alpha-tocopherol (αtoc) in membranes is to protect polyunsaturated lipids against oxidation. Although the chemistry of the process is well established, the role played by molecular structure that we address here with atomistic molecular-dynamics simulations remains controversial. The simulations were run in the constant particle NPT ensemble on hydrated lipid bilayers composed of SDPC (1-stearoyl-2-docosahexaenoylphosphatidylcholine, 18:0-22:6PC) and SOPC (1-stearoyl-2-oleoylphosphatidylcholine, 18:0-18:1PC) in the presence of 20 mol % αtoc at 37°C. SDPC with SA (stearic acid) for the *sn*-1 chain and DHA (docosahexaenoic acid) for the *sn*-2 chain is representative of polyunsaturated phospholipids, while SOPC with OA (oleic acid) substituted for the *sn*-2 chain serves as a monounsaturated control. Solid-state ^{2}H nuclear magnetic resonance and neutron diffraction experiments provide validation. The simulations demonstrate that high disorder enhances the probability that DHA chains at the *sn*-2 position in SDPC rise up to the bilayer surface, whereby they encounter the chromanol group on αtoc molecules. This behavior is reflected in the van der Waals energy of interaction between αtoc and acyl chains, and illustrated by density maps of distribution for acyl chains around αtoc molecules that were constructed. An ability to more easily penetrate deep into the bilayer is another attribute conferred upon the chromanol group in αtoc by the high disorder possessed by DHA. By examining the trajectory of single molecules, we found that αtoc flip-flops across the SDPC bilayer on a submicrosecond timescale that is an order-of-magnitude greater than in SOPC. Our results reveal mechanisms by which the sacrificial hydroxyl group on the chromanol group can trap lipid peroxyl radicals within the interior and near the surface of a polyunsaturated membrane. At the same time, water-soluble reducing agents that regenerate αtoc can access the chromanol group when it locates at the surface.

INTRODUCTION

Alpha-tocopherol (αtoc) is the form retained by the human body of a structurally related group of phenolic compounds that make up vitamin E (1,2). It is a lipid soluble antioxidant that is an essential micronutrient. Symptoms of deficiency include, for example, neuromuscular abnormities (3). There is overall consensus that a major function of αtoc is to prevent the oxidation of polyunsaturated lipids that are particularly vulnerable to free radical attack in subcellular and plasma membranes (2,4–6). The chemistry is well established (7,8), but it remains to be seen whether a structural component exists in support of this role (5,9–11). Here we present molecular dynamics (MD) simulations that reveal αtoc is well designed to protect polyunsaturated lipids.

The molecular structure of αtoc consists of a chromanol headgroup that is methylated at all three of the available positions on a benzene ring and to which a 16-carbon saturated phytyl chain is attached at the opposite end (Fig. 1). A hydroxyl group on the benzene ring is responsible for antioxidant activity (7,8). This hydrophilic group usually sits near the aqueous interface, anchored to a membrane by the hydrophobic chain that extends toward the center (12,13). There it scavenges lipid peroxyl radicals that rise up to the surface from the interior of the membrane via conformational isomerization, terminating the chain reaction by which lipid peroxidation proceeds. The same location provides easy access to polar reducing agents that regenerate αtoc. PUFAs (polyunsaturated fatty acids) are an influential membrane constituent (14), notably DHA (docosahexaenoic acid, 22:6, with six double bonds). Their incorporation into phospholipids in plasma membranes has been proposed to be responsible for a vast array of health benefits attributed to dietary consumption of fish oils rich in PUFA (15–17). Moreover, PUFA are abundant in the phospholipids of neural membranes, and their depletion from these specialized membranes results in functional impairment (18,19). Extremely high disorder is the unique property that PUFAs possess and by which polyunsaturated phospholipids

Submitted February 25, 2015, and accepted for publication August 24, 2015.

*Correspondence: swassall@iupui.edu

Editor: Emad Tajkhorshid.

0006-3495/15/10/1608/11

http://dx.doi.org/10.1016/j.bpj.2015.08.032

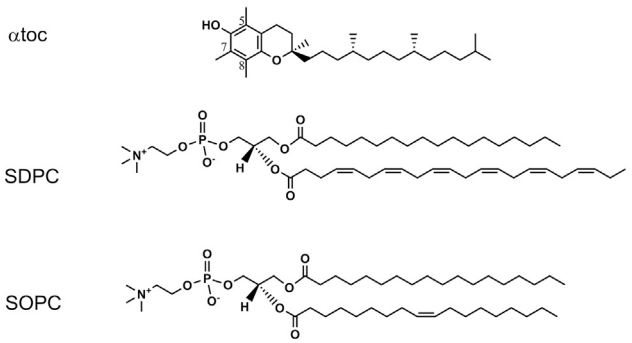

FIGURE 1 Molecular structure of αtoc, SDPC, and SOPC.

modulate membrane organization and protein activity (20–22). The origin of the disorder is the presence of a repeating =CH-CH_2-CH= unit within which the energy barrier to rotation about C-C bonds is shallow (23). Because the central methylene group in this recurring motif is readily attacked by free radicals (24), polyunsaturated phospholipids are prone to peroxidation and αtoc is thought to inhibit the process.

The amount of αtoc in membranes is extremely small. Reported levels are generally <1 mol % of the total lipid (25). Thus, polyunsaturated phospholipid molecules grossly outnumber the molecule that is meant to defend them from oxidation by a mechanism necessitating intimate contact. How αtoc can effectively do so in an encompassing milieu of lipids and proteins is unclear, and has led to proposals (as yet unproven) that it preferentially interacts with PUFA (9–11). Atomistic MD simulations have been integral in developing a detailed picture of polyunsaturated phospholipid bilayers in which PUFA chains rapidly isomerize between conformational states (26–28). In the current study, we applied this computational approach to compare the molecular organization of αtoc in SDPC (1-stearoyl-2-docosahexaenoylphosphatidylcholine, 18:0-22:6PC) and SOPC (1-stearoyl-2-oleoylphosphatidylcholine, 18:0-18:1PC) bilayers. SDPC with saturated SA (stearic acid, 18:0) for the *sn*-1 chain and DHA for the *sn*-2 chain is representative of a polyunsaturated phospholipid, while SOPC with OA (oleic acid, 18:1) containing a single double bond instead for the *sn*-2 chain serves as a monounsaturated control (Fig. 1). Solid state ^{2}H nuclear magnetic resonance (NMR) and neutron diffraction measurements were also performed to complement the MD simulations.

MATERIALS AND METHODS

MD simulations

MD simulations were performed for neat bilayers of SDPC and SOPC and of SDPC and SOPC containing 20 mol % αtoc. They were run in the constant particle, pressure, and temperature (NPT) ensemble. Each simulation has 100 lipid molecules and 2000 water molecules. The initial structures were assembled with the CHARMM-GUI Membrane Builder (29,30), and in presence of αtoc were prepared from the lipid-cholesterol structure built with CHARMM-GUI by replacing cholesterol with αtoc. Simulations were run using the CHARMM C36 (31) and C36p (32) force fields for SOPC and SDPC, respectively, with the customary cutoffs. Nonbonded (pairwise van der Waals and short-range electrostatic) interactions were smoothly turned off at 10 Å, while the particle-mesh Ewald method was employed to calculate long-range electrostatic interactions (33). The equilibration of bilayers was achieved using the standard CHARMM-GUI six-step process that gradually turns off restraints on lipids over 200 ps (30).

Production runs were over a minimum of 200 ns using a time step of 2 fs and the first 20 ns were considered as equilibration. The simulations were maintained in a rectangular box with equal x and y dimension (in the plane of the bilayer) and z varied independently in the NPT ensemble. The temperature was kept at 37°C by the Hoover thermostat (34) while the Nosé-Hoover piston was applied to keep the pressure at 1 atm (35). Analyses of simulations included the calculation of order parameters and neutron scattering length density (NSLD) profiles. The Lightweight Object-Oriented Structure (LOOS) library was employed to construct maps of the lateral distribution of lipid chains relative to αtoc (36). Snapshots of bilayers and plots of the maps of lateral distribution were created with the VISUAL MOLECULAR DYNAMICS program (37).

Solid-state ^{2}H NMR

Samples were aqueous multilamellar dispersions of 50 wt % lipid in 50 mM Tris buffer (pH 7.5). The lipids comprised SDPC-d_{35} (1-[$^2H_{35}$]stearoyl-2-docosahexaenoylphosphatidylcholine); SDPC-d_{35}/20 mol % αtoc; SOPC-d_{35} (1-[$^2H_{35}$]stearoyl-2-oleoylphosphatidylcholine); and SOPC-d_{35}/20 mol % αtoc. In each sample there was either 25 mg SDPC-d_{35} or SOPC-d_{35}. Avanti Polar Lipids (Alabaster, AL) was the source for the deuterated analogs of phospholipids, while deuterium-depleted water was purchased from Isotoec-Sigma-Aldrich (St. Louis, MO). αToc was obtained from commercial α-tocopheryl acetate by hydrolysis (K_2CO_3 in methanol for 5 h) and purification of the crude product via silica gel column chromatography using a step gradient of hexane/ether (95:5/9:1) as the eluting solvents. Preparation of the samples was as previously described in Marquardt et al. (38), with additional precautions outlined in earlier work taken due to the susceptibility of PUFAs to oxidation (39).

^{2}H NMR spectra were acquired on a homebuilt spectrometer operating at 46.0 MHz with a 7.05 T superconducting magnet (Oxford Instruments, Osney Mead, UK) (40) implementing a phase-alternated quadrupolar echo sequence ($90°_x$-τ-$90°_y$-acquire-delay)$_n$ (41). Data acquisition parameters were 90° pulse width = 3.8 μs; separation between pulses τ = 50 μs; delay between pulse sequences = 1.0 s; sweep width = ±100 kHz; dataset = 2 K; and number of transients = 10,000. The first moment M_1 was calculated from powder patterns obtained by conventional fast Fourier transform (FFT) and related to an average order parameter $\overline{S}_{CD}$ with standard equations (42). The FFT de-Paking algorithm was applied to produce the corresponding aligned spectra characteristic of a planar membrane (43). Exploiting the enhanced resolution of de-Paked spectra, profiles of order parameter S_{CD} were then constructed assuming the value of S_{CD} decreases smoothly along a lipid chain from the more ordered methylene groups near the membrane surface toward the disordered terminal methyl group in the middle of the membrane (44).

Neutron diffraction

Neutron diffraction of aligned multilayers prepared on a silicon single crystal substrate was employed to map the density distribution of lipid components along the membrane-normal (z) direction. The methods have been documented in Marquardt et al. (12). The samples comprised a total of 12 mg of SDPC or SOPC (Avanti Polar Lipids) with 20 mol % αtoc or a

labeled analog, α-[5-$^2H_3$]tocopherol (αtoc-d_3), having a deuterated methyl group at the 5-position on the chromanol group (Fig. 1). Preparation of the labeled analog was by a previously cited protocol (12). The bilayers were hydrated at fixed humidity using a saturated salt solution of KNO_3 (94% RH) with 70, 40, 16, and 8% ^2H_2O. Care was taken throughout sample manipulation and experimentation to minimize exposure to the atmosphere and light. Samples were kept at room temperature during initial equilibration and controlled at 37 ± 0.5°C during data collection.

Diffraction data were taken on the D3 beam-line at the Canadian Neutron Beam Center (Chalk River, Ontario, Canada). A wavelength of 2.37 Å was selected for the neutrons with a single crystal monochromator of pyrolytic graphite. Higher order (i.e., λ/2, etc.) reflections were eliminated using a pyrolytic graphite filter. Data correction and reconstruction of the bilayer profile proceeded as outlined in earlier work (12). Briefly, scattering form factors F_h were obtained from the integrated intensity of each of the quasi-Bragg peaks, typically 4–8, that were collected. The NSLD profile along the bilayer-normal z was derived with the cosine transformation of the form factors. The difference between the profiles for labeled and unlabeled samples was calculated from the transformation of the difference in their respective structure factors. Data were placed on an arbitrary scale for comparison with MD simulations.

RESULTS

Membrane organization and structure

Phospholipid acyl-chain order

The order parameter is defined according to

$$S_{CD} = \frac{1}{2}\langle 3\cos^2\beta - 1\rangle. \quad (1)$$

In this equation, β is the instantaneous angle between a C-H bond and the bilayer normal, about which lipid molecules reorient with axial symmetry, and the angular brackets designate a time average (45). The value of S_{CD} for a methylene or methyl group in a lipid chain is determined by the degree of anisotropy of the motion for the group and the profile of order parameter along a lipid chain is a sensitive indicator of membrane organization (46). From the MD simulations performed in this study we calculated order parameter profiles for the *sn*-1 and -2 chains in SDPC and SOPC both in the absence and presence of 20 mol % αtoc. We also determined smoothed-order parameter profiles for the *sn*-1 chain from the ^2H NMR spectra collected with SDPC-d_{35} and SOPC-d_{35}. Measurements made in ^2H NMR experiments are widely employed in validating MD simulations (47). Comparison between the two approaches, however, is not straightforward. NMR work is typically, as in this study, conducted at higher water content and in the presence of a buffer that can impact bilayer properties (48,49). Additionally, order parameters obtained experimentally are subject to instrumental factors that can distort the shape of the spectra from which they are evaluated (50,51).

Order parameter profiles along the *sn*-1 chain derived from MD simulations run on SDPC and SOPC bilayers at 37°C are plotted in Fig. 2 (*open squares* in *lower-left* and *-right panels*, respectively). The corresponding surface

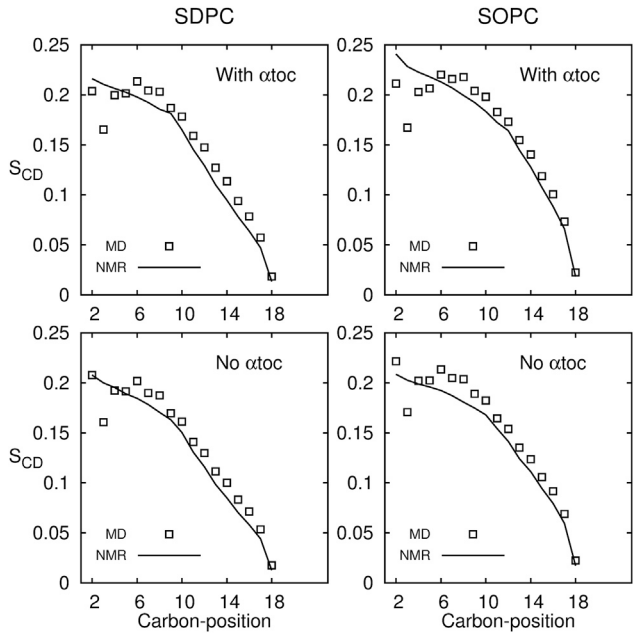

FIGURE 2 Order parameter profiles along the *sn*-1 chain in SDPC and SOPC at 37°C obtained from MD simulations (*open squares*) and FFT de-Paked ^2H NMR spectra (*continuous line*). (*Lower-left panel*, SDPC; *upper-left panel*, SDPC + 20 mol % αtoc; *lower-right panel*, SOPC; and *upper-right panel*, SOPC + 20 mol % αtoc). Fig. S2 shows the effect of αtoc on the order parameter profiles obtained from the MD simulations and ^2H NMR experiments separately. The uncertainty in the simulated data is $\leq \pm 2\%$, which was estimated from the standard error obtained treating each lipid molecule independently. A reproducibility of ±2% applies to the NMR data.

areas per lipid, together with the values in the presence of αtoc, are listed in Table S1 in the Supporting Material. In each case, the profile has the characteristic shape that is universally seen for a saturated chain esterified at the *sn*-1 position of phospholipids in the lamellar liquid crystalline phase. There is a plateau region of largely constant order parameter (S_{CD} ~ 0.2) in the upper-half of the chain near the bilayer surface followed by a progressive falloff in value in the lower half of the chain toward the disordered middle of the bilayer (46). Reflecting the much greater disorder possessed by DHA relative to OA in the adjacent *sn*-2 chain, order parameters are 10% lower on average in the SA chain of SDPC ($\overline{S}_{CD} = 0.137 \pm 0.003$) than SOPC ($\overline{S}_{CD} = 0.153 \pm 0.003$). When 20 mol % αtoc is added, the response is to increase order while maintaining the same overall shape for the profile along the SA chain in both SDPC ($\Delta\overline{S}_{CD} = 0.010$) and SOPC ($\Delta\overline{S}_{CD} = 0.008$) (*open squares* in *upper-left* and *-right panels*, respectively, in Fig. 2). This behavior is consistent with results published in earlier ^2H NMR studies on saturated and monounsaturated PC systems (38,52,53). The condensing effect of αtoc, not surprisingly, is more modest than seen with cholesterol (54,55). Although both molecules are comprised of rigid rings with a hydroxyl group at one end and a branched chain at the other, the chromanol group

on αtoc is approximately half the size of the steroid moiety on cholesterol.

The general trends seen in the profiles calculated from the MD simulations are corroborated by the order parameter profiles along the *sn*-1 chain constructed from ^{2}H NMR spectra collected using SDPC-d_{35} and SOPC-d_{35} (*continuous line* in the *left* and *right panels*, respectively) that are included in Fig. 2. SDPC-d_{35} ($\overline{S}_{CD} = 0.130 \pm 0.003$) is appreciably more disordered than SOPC-d_{35} ($\overline{S}_{CD} = 0.143 \pm 0.003$), and adding αtoc increases order in SDPC-d_{35} ($\Delta\overline{S}_{CD} = 0.011$) and SOPC-$d_{35}$ ($\Delta\overline{S}_{CD} = 0.015$). Because the profiles generated by NMR data are smoothed, it should be noted that subtleties in variation within the plateau region are not discerned. Copies of the de-Paked spectra from which the profiles were obtained can be found in Fig. S1 in the Supporting Material.

Order parameters calculated from the MD simulations along the *sn*-2 chain of SDPC and SOPC are shown in Fig. 3. In agreement with results from Gawrisch and Soubias (56), order parameters throughout almost all of the DHA chain in SDPC are very small ($S_{CD} < 0.05$) due to the high degree of flexibility associated with the multiple double bonds (*open circles* in *left panel*, Fig. 3). The S_{CD} values are comparable to the lowermost disordered portion of the SA chain at the *sn*-1 position. The profile for the OA chain in SOPC, by contrast, resembles that for the SA chain except there is a precipitous dip in the value of S_{CD} in the vicinity of the double bond (*open circles* in *right panel*, Fig. 3). Such a discontinuity is a feature of the order parameters obtained for an OA chain in phospholipid bilayers from ^{2}H NMR spectra (57) and computer simulations (58). An orientation resulting in intrinsically low S_{CD} values (not local segmental motion of large amplitude) is most likely responsible (57,59). Deviation from monotonic variation for the order parameter is evident as well at the C2 position where the values of S_{CD} for the two C-H bonds on the methylene group are

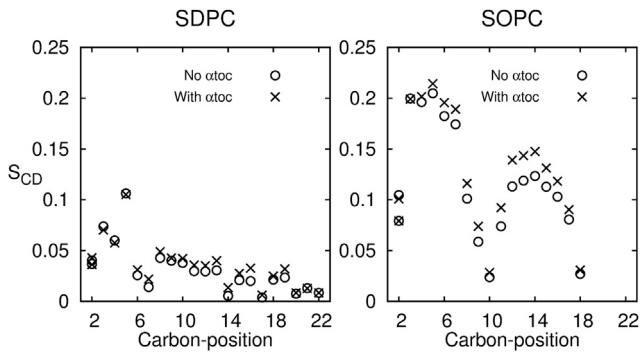

FIGURE 3 Order parameter profiles along the *sn*-2 chain in SDPC and SOPC at 37°C obtained from MD simulations. (*Left panel*) (*Open circles*) SDPC; (*X*) SDPC + 20 mol % αtoc. (*Right panel*) (*Open circles*) SOPC; (*X*) SOPC + 20 mol % αtoc.

depressed and unequal. It is attributed to constraints imposed by the glycerol backbone upon the initial orientation of the *sn*-2 chain (60).

An increase that is barely perceptible is revealed by the order parameters presented for the DHA chain in SDPC upon the introduction of 20 mol % αtoc (*crosses* in *left panel*, Fig. 3). The change in average value determined for order parameter ($\Delta\overline{S}_{CD} = 0.004$) is correspondingly very small. Minimal interference with the rapid transition between torsional states adopted by the polyunsaturated *sn*-2 chain due to αtoc is implied. Among the myriad of conformations formed (as identified in pioneering MD simulations on DHA-containing phospholipids (27)) are bent arrangements that bring much of the chain up to the membrane surface. How the OA chain in SOPC is affected by the addition of αtoc, has more in common with the situation for the SA chain. Like the SA chain, order parameters in the OA chain are elevated ($\Delta\overline{S}_{CD} = 0.013$) in a profile that retains the shape observed in the absence of αtoc (*crosses* in *right panel*, Fig. 3).

Location of α-tocopherol

Fig. 4 displays NSLD profiles for SDPC (*left*) and SOPC (*right*) bilayers containing 20 mol % αtoc computed from our MD simulations (*upper panel*). By assigning a neutron scattering length to each atom, they were generated with

$$\mathrm{NSLD} = \sum_i b_i n_i(z). \qquad (2)$$

Here z is the distance from the center of the membrane, b_i is the neutron scattering length for an atom of type i, and $n_i(z)$ is the number of atoms of type i in slices that are 0.2 Å thick. This format reveals structural information in a manner that is directly comparable to experiment. The distribution of the atoms on all the lipids (phospholipid and αtoc) about the midpoint of the bilayer ($z = 0$) has a negative dip at the middle that is due to the disordered methyl groups at the end of the lipid chains (*dashed line*). Scattering from the phosphate and glycero-ester regions is responsible for the symmetrically located maxima on each side. The separation of these maxima roughly represents the hydrocarbon thickness of the bilayer (61), which is 34.1 ± 0.3 Å for SDPC (*left-upper panel*) and 35.6 ± 0.4 Å for SOPC (*right-upper panel*). Consistent with the larger cross-sectional molecular area that accompanies higher disorder (Table S1), the bilayer is thinner for SDPC than SOPC. The scattering profile for only the deuterons, isotopic substituting for hydrogen, on the methyl group at the C5 position of the chromanol group in αtoc consists of a pair of peaks (*continuous line*). The peaks are ± 13.7 and ± 14.0 Å from the center of the bilayer in SDPC and SOPC, respectively. They are ~3–4 Å (3.3 ± 0.4 Å in SDPC and 3.8 ± 0.5 Å in SOPC) inside the maxima due to all atoms on the lipids in each case, which situates the chromanol group just below the

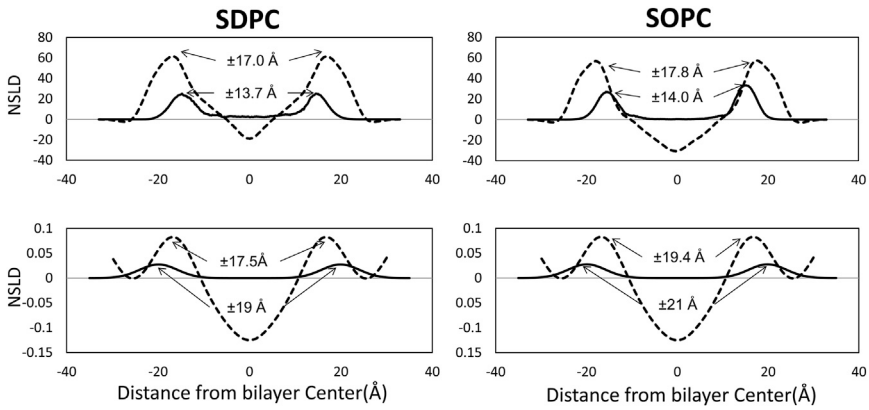

FIGURE 4 Neutron scattering length density (NSLD) profiles for SDPC+ 20 mol % αtoc (*left*) and SOPC + 20 mol % αtoc (*right*) at 37°C obtained from MD simulations (*upper panel*) and neutron diffraction experiments (*lower panel*). (*Dashed line*) Profile for all lipids (phospholipid and αtoc); (*solid line*) profile for deuterium on the C5 position of the chromanol group in αtoc (amplified in intensity for comparison). The uncertainty in the location of the center of the peak for the C5 position is ±0.3 Å in SDPC and SOPC (MD simulations), and ±1.5 Å in SDPC and ±1.0 Å in SOPC (neutron diffraction experiments).

membrane surface in SDPC and SOPC and is consistent with hydrogen bonding to the carbonyl groups on the phospholipids. This location falls within a range of sites in the vicinity of the aqueous interface that has been identified for a number of phospholipids by a variety of experimental techniques as well as computer modeling (12,13,25,62).

The MD simulations reproduce the chief features of the results from neutron diffraction measurements on aligned multilayers of SDPC (*left*, *lower panel*) and SOPC (*right*, *lower panel*) with 20 mol % αtoc (see Fig. 4).That a reduced level of hydration applies to the experiments (~11–15 water molecules/lipid) relative to the simulations (~20 water molecules/lipid), should be borne in mind. A separation of 35.0 ± 1.6 Å in SDPC and 38.8 ± 0.2 Å in SOPC applies to the maxima that flank the negative dip at the center of the NSLD profiles for the whole bilayer (*dashed line*) obtained by analyzing the neutron diffraction peaks (Fig. S3). In these profiles the contribution from water was suppressed by conducting the experiments with water that contained 8% $^{2}H_2O$ (61). The pair of peaks identified from the difference between NSLD profiles evaluated with bilayers prepared with labeled (αtoc-5d_3) and unlabeled αtoc (Fig. S4 and Table S2), places the C5 position on αtoc at ±19.0 and ±21.0 Å with respect to the center of the bilayer in SDPC and SOPC, respectively (*continuous line*). They lay ~2 Å (1.5 ± 2.0 Å in SDPC and 1.6 ± 1.0 Å in SOPC) outside the maxima due to the entire lipid in both cases, such that the chromanol group slightly protrudes into the phospholipid headgroup region, which suggests that there is hydrogen bonding to the phosphate group. Like the data from the MD simulations, although differences in detail exist, the experimental observations confirm that the chromanol group resides near the aqueous surface in SDPC and SOPC and imply that there is no appreciable disparity between the depth of αtoc in the polyunsaturated and monounsaturated systems.

The reason for the apparent discrepancy in position within the bilayer determined for αtoc from the analyses of our computational and experimental results is not entirely evident. Both approaches have inherent limitations, in common with NMR and other methods, and probe a system under conditions that are not identical. The MD simulations, the accuracy of which fundamentally depends on the reliability of the force field employed, were run on a patch containing 100 lipid molecules in a single bilayer. The neutron diffraction experiments, which rely crucially on the precise scaling of measurements made on two independent samples that differ only in isotopic replacement of deuterium for hydrogen at a specific molecular site, were performed on aligned multilayers on a silicon crystal substrate prepared, as noted above, at lower hydration.

Exactly where αtoc sits, moreover, cannot be surmised from the literature that has been published to date. Three basic models, which were comprehensively discussed in a subsequent review (25), have been proposed (63). They have the chromanol group poking into the headgroup region, recessed within the interfacial region and submerged into the bilayer. Each one has experimental support (25). The majority of the earlier reports, albeit often somewhat qualitative and/or subject to perturbation problems associated with the use of an extrinsic probe molecule, favor the latter two models. A location at the surface or within the bilayer was concluded on the basis of the quenching of the intrinsic fluorescence of αtoc produced by nitroxyl or anthroyloxyl stearic acids incorporated into DPPC (1,2-dipalmitoylphosphatidylcholine, 16:0-16:0PC) and egg PC (phosphatidylcholine) vesicles (64,65), the time course of the loss in intensity for ^{19}F NMR signals from ^{19}F-labeled analogs of αtoc in egg PC vesicles after the addition of Pr^{3+} (66), and the chemical shift-polarity correlation of ^{13}C NMR resonances for αtoc in DMPC (1,2-dimyristoylphosphatidylcholine, 14:0-14:0PC) vesicles (67). Close to the phosphate, the dissenting view that has the chromanol group in the polar region of the phospholipid headgroups, was deduced from lanthanide-induced shifts of ^{13}C NMR spectra observed for a ^{13}C-enriched analog of αtoc in egg PC vesicles (68).

Although providing more quantitative information, the MD simulations and neutron scattering work that have been described more recently only compound the debate. Just as in this investigation, the tendency is for the respective methods

to place the chromanol group on opposite sides of the lipid-water interface. Just beneath the interface was indicated in the computer simulations conducted on saturated and monounsaturated PC bilayers (62,69). Above and within the interfacial region was found in the neutron diffraction experiments done on saturated, monounsaturated, and polyunsaturated PC multilayers (12), although a dependence upon headgroup causing deeper penetration in POPS (1-palmitoyl-2-oleoylphosphatidylserine) was observed as well (13). That quite different water contents were employed should again be recognized when comparing the two types of result. It is impossible, additionally, to discern a pattern in the variation in placement determined for the chromanol group by the neutron-scattering measurements. As an example, substantially above, versus slightly below, the lipid-water interface was seen in POPC (1-palmitoyl-2-oleoylphosphatidylcholine, 16:0-18:1PC) and DOPC (1,2-dioleoylphosphatidylcholine, 18:1-18:1PC), which is the reverse of the trend seen in PAPC (1-palmitoyl-2-arachidonylphosphatidylcholine, 16:0-20:4PC) and its more disordered, homo-acid counterpart DAPC (1,2-diarachidonylphosphatidylcholine, 20:4-20:4PC) (12). Neutron-scattering data that has also been reported showing αtoc sequestering at the center of DMPC bilayers, further illustrate how poorly the situation is understood (38). A systematic attack on this problem will clearly be necessary in the future to resolve the issue.

Interaction of α-tocopherol with phospholipid acyl chains

To probe the relative affinity of αtoc for SDPC versus SOPC, the van der Waals (vdW) interaction energy between αtoc and phospholipid acyl chains and the density of each chain surrounding αtoc molecules was determined from the MD simulations.

vdW interaction energy

The vdW interaction energy was calculated in CHARMM by summing over pairs of nonbonded atoms using the standard Lennard-Jones potential,

$$U_{\mathrm{vdW}} = \sum_{ij} \varepsilon_{ij} \left[\left(\frac{R_{\min,ij}}{r_{ij}} \right)^{12} - \left(\frac{R_{\min,ij}}{r_{ij}} \right)^{6} \right], \qquad (3)$$

where ε_{ij} and $R_{\min,ij}$ are the energy and separation between pairs of atoms ij at equilibrium, respectively; and r_{ij} is the distance between the atoms (31). Fig. 5 shows the results for αtoc in SDPC (*upper*) and SOPC (*lower*) in the form of a bar graph. Separate values of U_{vdW} describing the interaction with the *sn*-1 and -2 chains are plotted. They reveal that the vdW interaction energy of αtoc with the saturated SA chain at the *sn*-1 position is less in SDPC (−20.3 kcal/mol) than SOPC (−23.4 kcal/mol), which we ascribe to the enhanced disorder, and hence loose packing,

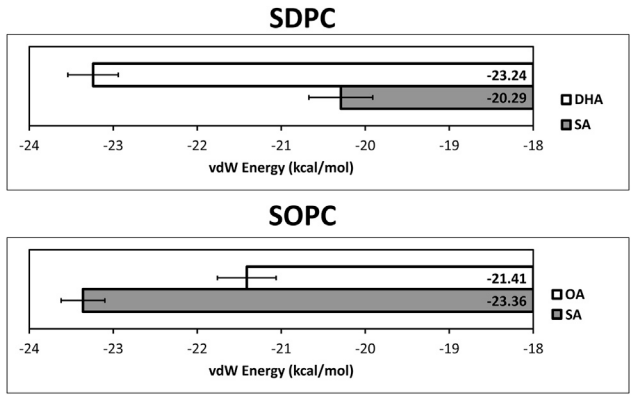

FIGURE 5 vdW energy for the interaction of αtoc with the *sn*-1 chain (*shaded bar*) and *sn*-2 chain (*open bar*) of the phospholipid in SDPC + 20 mol % αtoc (*upper panel*) and SOPC + 20 mol % αtoc (*lower panel*). The values plotted are an average over time for all αtoc molecules, and the errors were calculated based on the values for each αtoc molecule.

within the polyunsaturated bilayer. The opposite situation applies to the interaction of αtoc with the unsaturated chains at the *sn*-2 position. The vdW energy for the DHA chain in SDPC (−23.2 kcal/mol) exceeds that for the OA chain in SOPC (−21.4 kcal/mol). Moreover, the value of U_{vdW} for DHA is larger than SA in SDPC whereas it is smaller for OA than SA in SOPC. We attribute the greater proximity to αtoc implied for the polyunsaturated chain, paradoxically, to the tremendously high conformational freedom it possesses compared to a monounsaturated chain. Maps of the density of each chain around αtoc molecules constructed from the simulations provide insight into our explanation.

Spatial distribution of sn*-1 and -2 chains*

To better understand the interaction with the different chains in SDPC and SOPC, maps of the density of carbon atoms on the *sn*-1 and -2 chains surrounding αtoc molecules were generated utilizing the LOOS analysis library (36). In our examination the rigid chromanol group serves as the molecular frame of reference and a vector extending from positions C4 to C6 specifies the orientation relative to the bilayer normal. The population distributions for this vector calculated from our simulations possess a maximum, representing the most probable orientation, at 39° in SDPC and 35.5° in SOPC. A state for an αtoc molecule closely matching the most probable orientation in a bilayer was then selected from our simulations and for each αtoc molecule in every frame of trajectory, the entire system was translated and rotated so that all of the chromanol groups were aligned with this reference. Next, summing over the realigned trajectories, we mapped the probability density for the *sn*-1 and -2 chains of either SDPC or SOPC separately within a cube of 30 × 30 × 30 $\mathrm{Å}^3$ lying in the plane of the bilayer in the reference system with an origin at the center of mass of the chromanol group. The cube was divided into 1 × 1 × 1 $\mathrm{Å}^3$ bins, and the probability density ρ is

proportional to the number of times the carbon atoms in each chain appear in a bin during the 180 ns of simulation time.

In Fig. 6, the difference in spatial distribution of the *sn*-1 and -2 chains in SDPC (*left column*) and SOPC (*right column*) relative to αtoc is explored. For this purpose we have defined the parameter

$$\Delta\rho = \rho_2 - \rho_1, \tag{4}$$

where the subscripts specify the probability density for the respective chains. Two slices separated by ~10 Å in depth coinciding with the chromanol group (slice *A*) and well below within the phytyl side chain (slice *B*) are shown. They are color-coded contour maps in which $\Delta\rho > 0$ indicates a higher probability density for the *sn*-2 chain whereas $\Delta\rho < 0$ indicates a higher probability density for the *sn*-1 chain. There is a small central region where $\Delta\rho = 0$ that corresponds to the location of the chromanol group in slice *A*. Such a region is absent in slice *B*, which does not intersect with the chromanol group. In the case of SDPC, it is clear from slice *A* that around the chromanol group the probability of finding DHA (*sn*-2 chain) substantially exceeds SA (*sn*-1 chain). Lower down in the bilayer at slice *B*, the probability of more DHA than SA is no longer found and a largely uniform probability distribution exists across the entire slice. The situation differs in SOPC. Only a small differential exists between the probability of finding OA (*sn*-2 chain) and SA (*sn*-1 chain) around the chromanol group in slice *A*. In slice *B*, there is more SA than OA throughout.

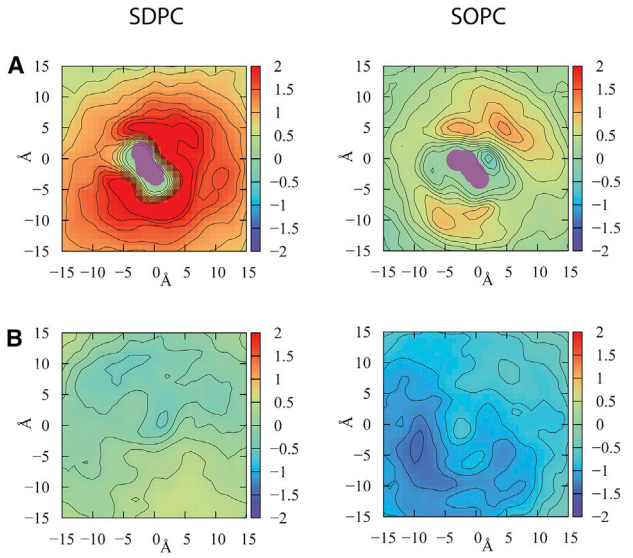

FIGURE 6 Color-coded contour maps of the difference in probability density ($\Delta\rho = \rho_2 - \rho_1$) for the carbons on the *sn*-1 and -2 chains in SDPC and SOPC around αtoc. The unit for ρ is the number of carbons counted in $1 \times 1 \times 1$ Å^3 bins over 180 ns of simulation. The densities were generated in a $30 \times 30 \times 30$ Å^3 cube centered on αtoc. Two representative slices lying in the *x*,*y* plane (parallel to the membrane surface) at different depths are shown. Slice (*A*) intersects the chromanol group while slice (*B*) lays ~10 Å below. To place the scales for $\Delta\rho$ in context, the respective average values for ρ_1 and ρ_2 in slice (*A*) are 3.95 and 5.15 for SDPC and 3.97 and 4.35 for SOPC, and in slice (*B*) are 4.74 and 4.79 for SDPC and 4.97 and 4.01 for SOPC.

The higher probability that DHA will be near the chromanol group can be explained in terms of the tremendous flexibility of the polyunsaturated chain, which leads to very low order parameters ($S_{CD} < 0.05$) throughout the entire DHA chain that are minimally perturbed by the presence of αtoc in SDPC (Fig. 3). With the exception of the very top portion, the DHA chain in SDPC moves through all conformational space in 50 ns (70). A greater density for DHA near the membrane surface, as opposed to the more rigid SA chain that has greater density in the middle of the membrane, is the result (71). This arrangement ensures that all parts of the DHA chain frequently approach the hydroxyl group on the chromanol group that is responsible for the antioxidant function of αtoc.

Flip-flop of α-tocopherol

Fig. 7 uncovers another aspect of the behavior of αtoc in a polyunsaturated environment with potential significance for the role of vitamin E as an antioxidant. In this figure, the trajectory in the transbilayer (*z*) direction for the C5 position on the chromanol group of one of the αtoc molecules in the SDPC bilayer is plotted over 60 ns of simulation. The plot demonstrates that, although the chromanol group

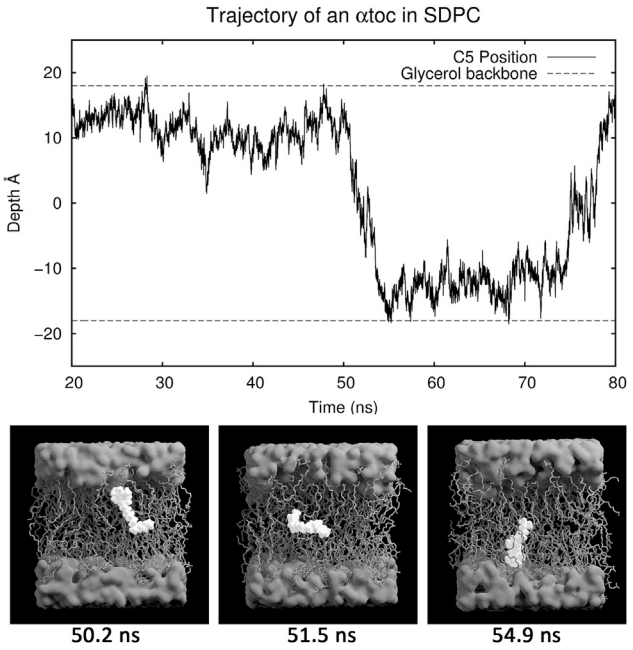

FIGURE 7 Trajectory in the transbilayer (*z*) direction of a representative αtoc molecule (*continuous line*, depth of C5 position on chromanol group) in SDPC (*dashed line*, location of glycerol backbone). Flip-flop of αtoc back and forth across the bilayer occurs at 50 and 75 ns. The three snapshots illustrate how the flip-flop occurs in a short time (~5 ns). An enlarged version of the snapshots may be found in Fig. S5.

usually sits at its canonical depth near the aqueous interface, the αtoc molecule also undergoes flip-flop across the bilayer. At ~50 ns the C5 position jumps from one side of the bilayer to the other and subsequently back at ~75 ns. The jumps are abrupt, ~5 ns in duration. During them, as illustrated in three snapshots taken during the first jump (Fig. 7), the αtoc molecule adopts short-lived conformations that include lying in the middle of the bilayer approximately parallel to the plane. A total of 22 flip-flops were counted throughout 180 ns for all 20 αtoc molecules in the bilayer, from which a lifetime of 0.16 μs (equivalent to half-life $t_{1/2} = 0.11$ μs) in SDPC was estimated. This rate is >10 times faster than in SOPC where only two flip-flops of αtoc molecules, corresponding to a lifetime of 1.8 μs ($t_{1/2} = 1.2$ μs), transpired under the same circumstances.

Flip-flop of phospholipids across protein-free membranes has long been recognized to be extremely slow (72). Passage through the hydrophobic interior is energetically unfavorable for the hydrophilic headgroups. A timescale of hours applies to the half-lives that have been measured by a variety of techniques, with the values depending upon headgroup and chain composition (73,74). Half-lives of 0.29 and 11.5 h describe the flip-flop of fluorescently labeled NBD-PE (7-nitrobenz-2-oxa-1,3-diazol-4-yl phosphatidylethanolamine) in SDPC and SOPC bilayers, respectively, at 25°C (74). They represent an increase in rate by a factor of 40× for the polyunsaturated membrane.

Very little attention has been paid to the flip-flop of αtoc. Estimates of the rate have been gleaned from only a sparse collection of MD simulations and experiments. There is an enormous discrepancy in the literature between the values according to these two approaches. Like in this work, translocation of αtoc from one leaflet to the other that was observed in recently published simulations runs for ~200 ns on several phospholipid bilayers in a highly fluid state at 350 K (62,69). A timescale of hours or longer, quite the reverse, was inferred in experimental studies conducted three decades ago monitoring the exchange of αtoc between the inner and outer layers of sonicated unilamellar vesicles (75,76). In our hands, however, assays of the oxidation of αtoc in PC vesicles showed complete loss of a fluorescence signal from αtoc on both sides of the bilayer in only a few minutes after the addition of potassium ferricyanide (unpublished data). There was no hint of long-term rate limitation brought about by flip-flop from the inner to outer leaflet. The very slow speed of transmembrane migration indicated for αtoc by the early work is difficult to understand. Methyl groups on either side (positions 5 and 7) shield the hydroxyl group in the chromanol moiety (Fig. 1), which should help overcome the energy barrier to movement through the hydrophobic core of the membrane. MD simulations on δ-tocopherol (δtoc), where neither position next to the hydroxyl group is methylated, support this notion in SDPC. There were only two flip-flops over 180 ns for δtoc in simulations that we ran under conditions identical to those on αtoc. Why flip-flop of αtoc should be much slower than cholesterol, in which seconds characterize the process (77), is also a mystery. Both molecules are structurally similar, composed of a rigid headgroup possessing a hydroxyl group at one end and a branched hydrocarbon chain at the opposite end.

DISCUSSION

αToc is the form of vitamin E that is a required component in the human diet. The primary function of this lipophilic antioxidant is to protect lipids, especially polyunsaturated phospholipids, in membranes against oxidation (78,79). To accomplish this purpose it traps a lipid peroxyl radical to break a chain of reactions that, once initiated, can oxidize many lipid molecules, and is subsequently restored by a water-soluble reducing agent such as ascorbate. Here we have performed for the first time, to our knowledge, atomistic MD simulations on the molecular organization of αtoc in a polyunsaturated phospholipid membrane. SDPC and SOPC bilayers in the absence and presence of 20 mol % αtoc were compared. SDPC is a polyunsaturated phospholipid that is representative of lipid species most susceptible to oxidative attack, while SOPC serves as a monounsaturated control that is much less vulnerable to such an assault.

The simulations capture the essence of the results from solid-state ^{2}H NMR and neutron diffraction experiments that were carried out to provide validation. The same distinctive shape defines the variation of order parameter along the SA chain at the *sn*-1 position in SDPC and SOPC obtained from the simulations and by analysis of ^{2}H NMR spectra (Fig. 2). There is a plateau region of essentially uniform order in the upper portion of the chain and then, in the lower portion, order drops off progressively more quickly toward the terminal methyl group. In line with the NMR-derived data, the profiles generated in silico demonstrated that SDPC is much more disordered than SOPC while the introduction of αtoc increases order by comparable amounts in both SDPC and SOPC. In accordance with the neutron diffraction measurements, the location of maxima attributable to the phosphate and glycerol-ester regions in the NSLD profile calculated from MD simulations showed that the thickness of the bilayer for SDPC is smaller than SOPC (Fig. 4). Both methods also placed the C5 position on the chromanol group of αtoc near the aqueous interface in the two membranes.

By comparing SDPC and SOPC bilayers, our simulations reveal aspects of molecular organization that help αtoc prevent the oxidation of polyunsaturated phospholipids. The extraordinary disorder possessed by PUFA chains, which promote contact with the sacrificial hydroxyl group on the chromanol moiety, is key. The extremely low order parameters that characterize the profile of order along the DHA chain at the *sn*-2 position in SDPC (Fig. 3) are indicative

of a rapidly varying conformation that redistributes the lower portion toward the bilayer surface (71,80). There is consequently, as depicted in maps of acyl-chain density generated from the simulated data (Fig. 6), increased likelihood that polyunsaturated chains reside in the immediate vicinity of the chomanol group on αtoc molecules. It is also apparent, from plots of trajectories in the transbilayer direction, that αtoc flip-flops across the bilayer in SDPC on a submicrosecond timescale (Fig. 7), which is >10 times more often than seen in SOPC. The frequent tunneling of αtoc through the fluid interior of an SDPC bilayer further enhances the chance that a chromanol group meets a polyunsaturated chain.

The findings from the MD simulations presented in this study, taken together, provide unprecedented structural insight into the molecular mechanism by which αtoc can efficiently inhibit the oxidation of polyunsaturated phospholipids in a membrane. They demonstrate how the hydroxyl group on the chromanol moiety, the reducing group in αtoc, is readily accessible to a lipophilic peroxyl radical formed anywhere within a PUFA chain and to water-soluble radicals that are necessary to restore antioxidant activity. The majority of the time the chromanol group sits near the membrane surface where water-soluble radicals easily reach it and intrinsic disorder brings even the lowest portion of polyunsaturated chains into close proximity on a regular basis. Flip-flop of αtoc, in addition, carries the chromanol group into the membrane interior and then back to the surface. This motion is made easier by loosely packed PUFA chains and by methyl groups at adjacent positions on the chromanol moiety that screen the hydroxyl group from the hydrophobic environment within a bilayer. It is emphasized that αtoc does not directly protect PUFA, but instead interacts with free radical intermediates formed during the series of reactions by which peroxidation proceeds. Our interpretation assumes that oxidized lipid chains retain high conformational mobility, which is implied by earlier work (81).

The situation is obviously more complex in a biological membrane. Because the concentration of αtoc is small, typically in the range of 0.1–1.0 mol % total phospholipid (25), lateral distribution relative to polyunsaturated phospholipids is another issue that affects its efficacy as an antioxidant. We have postulated that αtoc clusters with polyunsaturated phospholipids in domains, thereby locally compensating for its overall scarcity (11,16). This arrangement would facilitate frequent encounters with lipid peroxyl radicals by the mechanisms identified here.

In summary, an understanding of the role molecular structure plays in αtoc stopping the oxidation of polyunsaturated phospholipids in membranes emerges from our MD simulations. The simulations on SDPC show that the chromanol group lies in wait to meet DHA chains that move up to the surface of the bilayer and, remarkably, travels down to the inside of the bilayer as well. Thus, mechanisms by which αtoc not only can intercept lipid peroxyl radicals at the surface of a membrane but can also patrol the inside of the membrane are identified. By predominantly sitting with the chromanol group near the membrane surface, moreover, access to water-soluble reducing agents, which recycle α-tocopheroxyl radicals formed when lipid peroxyl radicals are trapped, is assured. We conclude from our results that αtoc is a lipid-soluble antioxidant that is well designed to protect polyunsaturated phospholipids in cell membranes.

SUPPORTING MATERIAL

Five figures and two tables are available at http://www.biophysj.org/biophysj/supplemental/S0006-3495(15)00867-X.

AUTHOR CONTRIBUTIONS

X.L. performed research, analyzed data, and wrote the article; J.J.K. performed research and analyzed data; D.M. performed research and analyzed data; M.G. purified and synthesized material; N.K. performed research and analyzed data; J.K. analyzed data and contributed analytic tools; J.A. contributed material; T.A.H. analyzed data and contributed analytic tools; S.E.F. designed research, analyzed data, and contributed analytical tools; and S.R.W. designed research, analyzed data, and wrote the article.

ACKNOWLEDGMENTS

We thank Justin A. Williams for help with sample preparation and the Alan Grossfield group for advice with implementation of the LOOS library.

Funding was provided by the Indiana University-Purdue University Indianapolis Center for Membrane Biosciences (to S.R.W.), National Science Foundation grant No. MCB-0950258 (to S.E.F.), Natural Sciences and the Engineering Research Council of Canada Discovery Grant (to J.A.), and the Department of Energy Scientific User Facilities Division, Office of Basic Energy Sciences, under contract no. DEAC05-00OR2275 (to J.K.).

REFERENCES

1. Zingg, J. M. 2007. Vitamin E: an overview of major research directions. *Mol. Aspects Med.* 28:400–422.
2. Niki, E., and M. G. Traber. 2012. A history of vitamin E. *Ann. Nutr. Metab.* 61:207–212.
3. Ulatowski, L., and D. Manor. 2013. Vitamin E trafficking in neurologic health and disease. *Ann. Rev. Nutr.* 33:87–103.
4. Packer, L. 1994. Vitamin E is nature's master antioxidant. *Sci. Am. Sci. Med.* 1:54–63.
5. Wang, X., and P. J. Quinn. 1999. Vitamin E and its function in membranes. *Prog. Lipid Res.* 38:309–336.
6. Traber, M. G., and J. Atkinson. 2007. Vitamin E, antioxidant and nothing more. *Free Radic. Biol. Med.* 43:4–15.
7. Burton, G. W., and K. U. Ingold. 1986. Vitamin E: application of the principles of physical organic chemistry to the exploration of its structure and function. *Acc. Chem. Res.* 19:194–201.
8. Alessi, M., T. Paul, …, K. U. Ingold. 2002. The contrasting kinetics of peroxidation of vitamin E-containing phospholipid unilamellar vesicles and human low-density lipoprotein. *J. Am. Chem. Soc.* 124:6957–6965.
9. Diplock, A. T., and J. A. Lucy. 1973. The biochemical modes of action of vitamin E and selenium: a hypothesis. *FEBS Lett.* 29:205–210.

10. Kagan, V. E. 1989. Tocopherol stabilizes membrane against phospholipase A, free fatty acids, and lysophospholipids. *Ann. N. Y. Acad. Sci.* 570:121–135.
11. Atkinson, J., T. Harroun, …, J. Katsaras. 2010. The location and behavior of α-tocopherol in membranes. *Mol. Nutr. Food Res.* 54:641–651.
12. Marquardt, D., J. A. Williams, …, T. A. Harroun. 2013. Tocopherol activity correlates with its location in a membrane: a new perspective on the antioxidant vitamin E. *J. Am. Chem. Soc.* 135:7523–7533.
13. Marquardt, D., N. Kučerka, …, T. A. Harroun. 2015. α-Tocopherol's location in membranes is not affected by their composition. *Langmuir.* 31:4464–4472.
14. Stillwell, W., and S. R. Wassall. 2003. Docosahexaenoic acid: membrane properties of a unique fatty acid. *Chem. Phys. Lipids.* 126:1–27.
15. Salem, N., Jr., H.-Y. Kim, and J. A. Yergey. 1986. Docosahexaenoic acid: membrane function and metabolism. *In* Health Effects of Polyunsaturated Fatty Acids in Seafoods. A. P. Simopoulos, R. R. Kifer, and R. E. Martin, editors. Academic Press, New York, pp. 263–317.
16. Wassall, S. R., and W. Stillwell. 2009. Polyunsaturated fatty acid-cholesterol interactions: domain formation in membranes. *Biochim. Biophys. Acta.* 1788:24–32.
17. Shaikh, S. R. 2012. Biophysical and biochemical mechanisms by which dietary N-3 polyunsaturated fatty acids from fish oil disrupt membrane lipid rafts. *J. Nutr. Biochem.* 23:101–105.
18. Salem, N., Jr., B. Litman, …, K. Gawrisch. 2001. Mechanisms of action of docosahexaenoic acid in the nervous system. *Lipids.* 36:945–959.
19. Niu, S.-L., D. C. Mitchell, …, B. J. Litman. 2004. Reduced G protein-coupled signaling efficiency in retinal rod outer segments in response to *n*-3 fatty acid deficiency. *J. Biol. Chem.* 279:31098–31104.
20. Brown, M. F. 1994. Modulation of rhodopsin function by properties of the membrane bilayer. *Chem. Phys. Lipids.* 73:159–180.
21. Gawrisch, K., O. Soubias, and M. Mihailescu. 2008. Insights from biophysical studies on the role of polyunsaturated fatty acids for function of G-protein coupled membrane receptors. *Prostaglandins Leukot. Essent. Fatty Acids.* 79:131–134.
22. Shaikh, S. R., J. J. Kinnun, …, S. R. Wassall. 2015. How polyunsaturated fatty acids modify molecular organization in membranes: insight from NMR studies of model systems. *Biochim. Biophys. Acta.* 1848:211–219.
23. Feller, S. E. 2008. Acyl chain conformations in phospholipid bilayers: a comparative study of docosahexaenoic acid and saturated fatty acids. *Chem. Phys. Lipids.* 153:76–80.
24. Ingold, K. U., V. W. Bowry, …, C. Walling. 1993. Autoxidation of lipids and antioxidation by α-tocopherol and ubiquinol in homogeneous solution and in aqueous dispersions of lipids: unrecognized consequences of lipid particle size as exemplified by oxidation of human low density lipoprotein. *Proc. Natl. Acad. Sci. USA.* 90:45–49.
25. Atkinson, J., R. F. Epand, and R. M. Epand. 2008. Tocopherols and tocotrienols in membranes: a critical review. *Free Radic. Biol. Med.* 44:739–764.
26. Saiz, L., and M. L. Klein. 2001. Structural properties of a highly polyunsaturated lipid bilayer from molecular dynamics simulations. *Biophys. J.* 81:204–216.
27. Feller, S. E., K. Gawrisch, and A. D. MacKerell, Jr. 2002. Polyunsaturated fatty acids in lipid bilayers: intrinsic and environmental contributions to their unique physical properties. *J. Am. Chem. Soc.* 124:318–326.
28. Huber, T., K. Rajamoorthi, …, M. F. Brown. 2002. Structure of docosahexaenoic acid-containing phospholipid bilayers as studied by ^{2}H NMR and molecular dynamics simulations. *J. Am. Chem. Soc.* 124:298–309.
29. Jo, S., T. Kim, …, W. Im. 2008. CHARMM-GUI: a web-based graphical user interface for CHARMM. *J. Comput. Chem.* 29:1859–1865.
30. Jo, S., J. B. Lim, …, W. Im. 2009. CHARMM-GUI MEMBRANE BUILDER for mixed bilayers and its application to yeast membranes. *Biophys. J.* 97:50–58.
31. Klauda, J. B., R. M. Venable, …, R. W. Pastor. 2010. Update of the CHARMM all-atom additive force field for lipids: validation on six lipid types. *J. Phys. Chem. B.* 114:7830–7843.
32. Klauda, J. B., V. Monje, …, W. Im. 2012. Improving the CHARMM force field for polyunsaturated fatty acid chains. *J. Phys. Chem. B.* 116:9424–9431.
33. Darden, T., D. York, and L. Pedersen. 1993. Particle mesh Ewald: an *n*·log(*n*) method for Ewald sums in large systems. *J. Chem. Phys.* 98:10089–10092.
34. Hoover, W. G. 1985. Canonical dynamics: equilibrium phase-space distributions. *Phys. Rev. A.* 31:1695–1697.
35. Nosé, S., and M. L. Klein. 1983. A study of solid and liquid carbon tetrafluoride using the constant pressure molecular dynamics technique. *J. Chem. Phys.* 72:6928–6939.
36. Romo, T. D., and A. Grossfield. 2009. LOOS: an extensible platform for the structural analysis of simulations. *In* Proceedings of the 31st International IEEE EMBS Conference. Institute of Electrical and Electronics Engineers, Piscataway, NJ, pp. 332–2335.
37. Humphrey, W., A. Dalke, and K. Schulten. 1996. VMD: visual molecular dynamics. *J. Mol. Graph.* 14:33–38, 27–28.
38. Marquardt, D., J. A. Williams, …, T. A. Harroun. 2014. Dimyristoyl phosphatidylcholine: a remarkable exception to α-tocopherol's membrane presence. *J. Am. Chem. Soc.* 136:203–210.
39. Brzustowicz, M. R., V. Cherezov, …, S. R. Wassall. 2002. Molecular organization of cholesterol in polyunsaturated membranes: microdomain formation. *Biophys. J.* 82:285–298.
40. Williams, J. A., S. E. Batten, …, S. R. Wassall. 2012. Docosahexaenoic and eicosapentaenoic acids segregate differently between raft and non-raft domains. *Biophys. J.* 103:228–237.
41. Davis, J. H., K. R. Jeffrey, …, T. P. Higgs. 1976. Quadrupolar echo deuteron magnetic resonance spectroscopy in ordered hydrocarbon chains. *Chem. Phys. Lett.* 42:390–394.
42. Davis, J. H. 1983. The description of membrane lipid conformation, order and dynamics by ^{2}H-NMR. *Biochim. Biophys. Acta.* 737:117–171.
43. McCabe, M. A., and S. R. Wassall. 1997. Rapid deconvolution of NMR powder spectra by weighted fast Fourier transformation. *Solid State Nucl. Magn. Reson.* 10:53–61.
44. Lafleur, M., B. Fine, …, M. Bloom. 1989. Smoothed orientational order profile of lipid bilayers by ^{2}H-nuclear magnetic resonance. *Biophys. J.* 56:1037–1041.
45. Seelig, J. 1977. Deuterium magnetic resonance: theory and application to lipid membranes. *Q. Rev. Biophys.* 10:353–418.
46. Holte, L. L., F. Separovic, and K. Gawrisch. 1996. Nuclear magnetic resonance investigation of hydrocarbon chain packing in bilayers of polyunsaturated phospholipids. *Lipids.* 31 (*Suppl*):S199–S203.
47. Vermeer, L. S., B. L. de Groot, …, J. Czaplicki. 2007. Acyl chain order parameter profiles in phospholipid bilayers: computation from molecular dynamics simulations and comparison with ^{2}H NMR experiments. *Eur. Biophys. J.* 36:919–931.
48. Mallikarjunaiah, K. J., A. Leftin, …, M. F. Brown. 2011. Solid-state ^{2}H NMR shows equivalence of dehydration and osmotic pressures in lipid membrane deformation. *Biophys. J.* 100:98–107.
49. Koerner, M. M., L. A. Palacio, …, H. I. Petrache. 2011. Electrodynamics of lipid membrane interactions in the presence of zwitterionic buffers. *Biophys. J.* 101:362–369.
50. Bloom, M., J. H. Davis, and M. I. Valic. 1980. Spectral distortion effects due to finite pulse widths in deuterium nuclear magnetic resonance spectroscopy. *Can. J. Phys.* 58:1510–1517.
51. Schäfer, H., B. Mädler, and E. Sternin. 1998. Determination of orientational order parameters from ^{2}H NMR spectra of magnetically partially oriented lipid bilayers. *Biophys. J.* 74:1007–1014.
52. Wassall, S. R., J. L. Thewalt, …, R. J. Cushley. 1986. Deuterium NMR study of the interaction of α-tocopherol with a phospholipid model membrane. *Biochemistry.* 25:319–326.

53. Suzuki, Y. J., M. Tsuchiya, …, L. Packer. 1993. Structural and dynamic membrane properties of α-tocopherol and α-tocotrienol: implication to the molecular mechanism of their antioxidant potency. *Biochemistry.* 32:10692–10699.

54. Polozov, I. V., and K. Gawrisch. 2007. NMR detection of lipid domains. *Methods Mol. Biol.* 398:107–126.

55. Mihailescu, M., O. Soubias, …, K. Gawrisch. 2011. Structure and dynamics of cholesterol-containing polyunsaturated lipid membranes studied by neutron diffraction and NMR. *J. Membr. Biol.* 239:63–71.

56. Gawrisch, K., and O. Soubias. 2008. Structure and dynamics of polyunsaturated hydrocarbon chains in lipid bilayers—significance for GPCR function. *Chem. Phys. Lipids.* 153:64–75.

57. Seelig, J., and N. Waespe-Sarcevic. 1978. Molecular order in *cis* and *trans* unsaturated phospholipid bilayers. *Biochemistry.* 17:3310–3315.

58. Wassall, S. R., M. A. McCabe, …, S. E. Feller. 2010. Solid-state ^{2}H NMR and MD simulations of positional isomers of a monounsaturated phospholipid membrane: structural implications of double bond location. *J. Phys. Chem. B.* 114:11474–11483.

59. Soni, S. P., J. A. Ward, …, S. R. Wassall. 2009. Effect of *trans* unsaturation on molecular organization in a phospholipid membrane. *Biochemistry.* 48:11097–11107.

60. Engel, A. K., and D. Cowburn. 1981. The origin of multiple quadrupole couplings in the deuterium NMR spectra of the 2 chain of 1,2 dipalmitoyl-*sn*-glycero-3-phosphorylcholine. *FEBS Lett.* 126:169–171.

61. Harroun, T. A., J. Katsaras, and S. R. Wassall. 2006. Cholesterol hydroxyl group is found to reside in the center of a polyunsaturated lipid membrane. *Biochemistry.* 45:1227–1233.

62. Qin, S.-S., and Z.-W. Yu. 2011. Molecular dynamics simulations of α-tocopherol in model membranes. *Wuli Huaxue Xuebao.* 27:213–227.

63. Fukuzawa, K., W. Ikebata, …, S. Urano. 1993. Location of α-tocopherol in phospholipid vesicles and its dynamics in inhibiting lipid peroxidation. *In* Vitamin E: Its Usefulness in Health and in Curing Diseases. M. Mino, H. Nakamura, A. T. Diplock, and H. J. Kayden, editors. Japan Scientific Societies Press, Tokyo, Japan, pp. 31–40.

64. Bisby, R. H., and S. Ahmed. 1989. Transverse distribution of α-tocopherol in bilayer membranes studied by fluorescence quenching. *Free Radic. Biol. Med.* 6:231–239.

65. Gomez-Fernandez, J. C., J. Villalain, …, M. J. Prieto. 1989. Localization of α-tocopherol in membranes. *Ann. N. Y. Acad. Sci.* 570:109–120.

66. Urano, S., M. Matsuo, …, K. Fukuzawa. 1993. Mobility and molecular orientation of vitamin E in liposomal membranes as determined by ^{19}F NMR and fluorescence polarization techniques. *Arch. Biochem. Biophys.* 303:10–14.

67. Afri, M., B. Ehrenberg, …, A. A. Frimer. 2004. Active oxygen chemistry within the liposomal bilayer. Part III: locating vitamin E, ubiquinol and ubiquinone and their derivatives in the lipid bilayer. *Chem. Phys. Lipids.* 131:107–121.

68. Perly, B., I. C. P. Smith, …, K. U. Ingold. 1985. Estimation of the location of natural α-tocopherol in lipid bilayers by ^{13}C-NMR spectroscopy. *Biochim. Biophys. Acta.* 819:131–135.

69. Qin, S.-S., Z.-W. Yu, and Y.-X. Yu. 2009. Structural and kinetic properties of α-tocopherol in phospholipid bilayers, a molecular dynamics simulation study. *J. Phys. Chem. B.* 113:16537–16546.

70. Soubias, O., and K. Gawrisch. 2007. Docosahexaenoyl chains isomerize on the sub-nanosecond time scale. *J. Am. Chem. Soc.* 129:6678–6679.

71. Mihailescu, M., and K. Gawrisch. 2006. The structure of polyunsaturated lipid bilayers important for rhodopsin function: a neutron diffraction study. *Biophys. J.* 90:L4–L6.

72. Contreras, F.-X., L. Sánchez-Magraner, …, F. M. Goñi. 2010. Transbilayer (flip-flop) lipid motion and lipid scrambling in membranes. *FEBS Lett.* 584:1779–1786.

73. Homan, R., and H. J. Pownall. 1988. Transbilayer diffusion of phospholipids: dependence on headgroup structure and acyl chain length. *Biochim. Biophys. Acta.* 938:155–166.

74. Armstrong, V. T., M. R. Brzustowicz, …, W. Stillwell. 2003. Rapid flip-flop in polyunsaturated (docosahexaenoate) phospholipid membranes. *Arch. Biochem. Biophys.* 414:74–82.

75. Bellemare, F., and M. Fragata. 1981. Transmembrane distribution of α-tocopherol in single-lamellar mixed lipid vesicles. *J. Membr. Biol.* 58:67–74.

76. Tyurin, V. A., V. E. Kagan, …, T. S. Stoichev. 1986. Interaction of α-tocopherol with phospholipid liposomes: absence of transbilayer mobility. *Bull. Exp. Biol. Med.* 102:1677–1680.

77. Hamilton, J. A. 2003. Fast flip-flop of cholesterol and fatty acids in membranes: implications for membrane transport proteins. *Curr. Opin. Lipidol.* 14:263–271.

78. Niki, E. 2014. Role of vitamin E as a lipid-soluble peroxyl radical scavenger: in vitro and in vivo evidence. *Free Radic. Biol. Med.* 66:3–12.

79. Lebold, K. M., and M. G. Traber. 2014. Interactions between α-tocopherol, polyunsaturated fatty acids, and lipoxygenases during embryogenesis. *Free Radic. Biol. Med.* 66:13–19.

80. Eldho, N. V., S. E. Feller, …, K. Gawrisch. 2003. Polyunsaturated docosahexaenoic vs docosapentaenoic acid-differences in lipid matrix properties from the loss of one double bond. *J. Am. Chem. Soc.* 125:6409–6421.

81. Garrec, J., A. Monari, …, M. Tarek. 2014. Lipid peroxidation in membranes: the peroxyl radical does not "float". *J. Phys. Chem. Lett.* 5:1653–1658.